# High nitrogen and carbon isotopic ratios in the interstellar comet 3I/ATLAS

Opitom, C.[†1*], Manfroid, J.[†2], Hutsemékers, D.[†2], Jehin, E.[2], Knight, M. M.[3], Aravind, K.[2], Ferellec, L.[4], Bodewits, D.[5], Guzmán, V. V.[6], Cordiner, M.[7,8], Dorsey, R. C.[9], La Forgia, F.[10], Lippi, M.[11], Murphy, B. P.[1], Snodgrass, C.[1], Bannister, M.[12]

[1*]Institute for Astronomy, University of Edinburgh, Royal Observatory, Edinburgh EH9 3HJ, UK.

[2]STAR Institute, University of Liège, Allée du 6 août, 19, 4000 Liège (Sart-Tilman), Belgium.

[3]Volgenau Department of Physics, United States Naval Academy, 572C Holloway Road, Annapolis, MD 21402, USA.

[4]Faculty of Science and Engineering, Northumbria University, Newcastle NE1 8ST, UK.

[5]Physics Department, Edmund C. Leach Science Center, Auburn University, Auburn, AL 36849, USA.

[6]Instituto de Astrofísica, Pontificia Universidad Católica de Chile, Av. Vicu na Mackenna 4860, 7820436 Macul, Santiago, Chile.

[7]Department of Physics, Catholic University of America, Washington, DC 20064, USA.

[8]Astrochemistry Laboratory, NASA Goddard Space Flight Center, 8800 Greenbelt Road, Greenbelt, MD 20771, USA.

[9]Department of Physics, P.O. Box 64, 00014 University of Helsinki, Finland.

[10]Department of Physics and Astronomy, University of Padova, vicolo Osservatorio 3, 35020 Padova, Italy.

[11]INAF - Osservatorio Astrofisico di Arcetri, Largo Enrico Fermi 5, 50125 Firenze, Italy.

[12]School of Physical and Chemical Sciences – Te Kura Matū, University of Canterbury, Private Bag 4800, Christchurch, 8140, Aotearoa New Zealand.

---

[0†] These authors contributed equally to this work.

*Corresponding author(s). E-mail(s): copitom@ed.ac.uk;

**Abstract**

Interstellar objects provide a unique opportunity to further our understanding of the planetary formation process by studying in detail material formed around another star. Their ices contain precious clues about the environment and conditions prevailing in their home system. As fractionation processes can be sensitive to the temperature and radiation environment, isotopic ratios are powerful tracers of the origin and evolution of different species. While isotopic ratios have been measured in solar system comets, previously detected interstellar objects have been too faint to measure isotopic ratios. Here we report the measurement of two ratios in 3I/ATLAS from observations of the CN molecule: $^{12}$C/$^{13}$C and $^{14}$N/$^{15}$N. We report $^{12}$C/$^{13}$C = $\mathbf{151}^{+110}_{-44}$ and $^{14}$N/$^{15}$N = $\mathbf{363}^{+633}_{-153}$. The $^{14}$N/$^{15}$N is higher than the value of $\sim$ 150 usually measured for solar system comets, close to the values measured in the interstellar medium, pre-stellar phases or the outside of protoplanetary discs. The $^{12}$C/$^{13}$C is higher than the values usually measured for solar system comets and in the local interstellar medium. These measurements are compatible with an origin of 3I in the outer disc around an older low-metallicity star.

**Keywords:** 3I/ATLAS, Interstellar object, Composition, Isotopic ratio, comet

Interstellar objects, formed in planetary systems beyond our own and now passing through the solar system, provide a rare opportunity to study material formed in another protoplanetary disc potentially having very different physical and chemical conditions. When such objects become active and sublimate, the released gases can be studied spectroscopically, allowing us to directly probe their volatile composition and isotopic ratios. While modern instrumentation allows us to study protoplanetary discs remotely, their large distances from us constrain the level of detail that can be obtained. By contrast, studying interstellar objects at a relatively close distance while they are passing through the solar system provides a unique window into the conditions prevailing in these discs where planetesimals and planets are forming. The composition of their ices, and especially the relative abundances of isotopes, constitute invaluable probes into their formation conditions.

The first two interstellar objects, 1I/'Oumuamua, discovered in 2017 [1] and 2I/Borisov discovered in 2019[1] (hereafter 1I and 2I, respectively), were studied intensively by astronomers all around the world. However, no gas was detected around 1I and the constraints put on the composition of 2I were limited by its relatively low brightness.

3I/ATLAS (hereafter 3I) was discovered in July 2025 by the ATLAS survey at about 5 au from the Sun and already active [2–5]. 3I was discovered several months before its perihelion which occurred on 29th October 2025 and was significantly

[1] *Minor Planet Electronic Circular* 2023-U162

brighter than previously discovered interstellar objects. Early observations indicated that 3I may have a composition different from that of most solar system comets. JWST observations at 3.3 au pre-perihelion revealed a coma extremely rich in $CO_2$ and to a lesser degree CO, relative to water [6]. Further measurements post-perihelion when 3I was at 2.4 au show a lower $CO_2/H_2O$ and slightly higher $CO/H_2O = 2.33 \pm 0.07$ compared to pre-perihelion measurements [7]. These post-perihelion ratios are high compared to the average comet observed at this distance from the Sun [8]. High spectral-resolution optical observations unveiled a very high nickel abundance and, once the comet approached perihelion, the presence of iron in the coma, with a Ni I/Fe I abundance ratio initially exceeding that observed in solar system comets [9, 10]. In addition, [11] reported an exceptionally high $CH_3OH/HCN$ ratio, higher than measured in all but one solar system comet.

Together, these compositional signatures suggest that 3I formed under conditions markedly different from those that prevailed in the Solar System. Isotopic ratios are often used to trace the origin and evolution of different species. As fractionation processes are sensitive to the temperature and radiation environment, isotopic ratios allow us to follow the chemical evolution of material from the pre-stellar stage, through the protostellar and protoplanetary disc stages, and into fully formed planets and planetesimals. As such, isotopic ratios provide a very sensitive probe of the formation conditions. Within the solar system, isotopic ratios of C, N, O, and H have been measured in a wide range of bodies, revealing substantial variations measured for D/H or $^{14}N/^{15}N$, e.g. [12].

Nitrogen isotope ratios are particularly diagnostic as they can be significantly modified by disc chemistry, especially through isotope-selective photo-dissociation which is dependent on the radiative environment within the disc as well as its physical and chemical structure. Early models proposed that nitrogen isotope fractionation was primarily driven by isotope exchange reactions [13], but recent investigations have shown that these reactions are much less efficient than originally thought [14]. An alternative mechanism involves the isotope-selective photo-dissociation of $N_2$ and the subsequent formation of species enriched in $^{15}N$, including HCN [12]. At small distances from the star, high $N_2$ abundances and strong UV radiation lead to $N_2$ self-shielding. This effect favours the photodissociation of $N^{15}N$, lowering $^{14}N/^{15}N$ ratios in the inner disc. This is consistent with the trend of increase in $^{14}N/^{15}N$ ratios with the stellar distance measured from observations of HCN in protoplanetary discs [15, 16].

The ratio between the two stable nitrogen isotopes ($^{14}N/^{15}N$) has been measured in a range of solar system comets, using different molecular tracers. Observations of CN revealed an enrichment in heavy nitrogen by a factor of three relative to proto-solar value [17]. Similar enrichments were subsequently found in HCN and later in $NH_2$, see the review in [18]. In situ measurements by the ROSINA mass spectrometer on board Rosetta determined $^{14}N/^{15}N \sim 130$ in molecular nitrogen in comet 67P/Churyumov-Gerasimenko [19]. This value is consistent with what is measured from observations of CN, HCN and $NH_2$ for other comets, thus ruling out the hypothesis of the existence of two distinct nitrogen reservoirs in comets. Overall, the measured values are remarkably uniform across solar system comets of different dynamical origins. One notable

exception is the lower heavy nitrogen enrichment in split comet 73P/Schwassmann-Wachmann 3 (hereafter 73P) [17]. More recently, [20] reported a $^{14}N/^{15}N$ ratio of $68 \pm 27$ in comet 46P/Wirtanen (hereafter 46P) from HCN observations, suggesting a larger diversity of nitrogen fractionation among solar system comets than originally thought. However, independent measurements of CN in the same comet yielded a value of $150 \pm 30$ [21], consistent with what is measured for most solar system comets. This discrepancy is surprising, as CN is thought to be produced mainly (even if not exclusively) by the photodissociation of HCN [22]. We would then expect the same ratios to be measured for both species for a given object. Indeed, for other solar system comets, both carbon and nitrogen ratios measured in CN and HCN usually agree within the uncertainties (see Tables 3 and 4). With the exception of 46P, this is true both at the individual object level as well as for whole population averages. Modelling in molecular clouds also suggests very similar ratios for both species [23]. The origin of the $^{15}N$ enrichment in solar system comets remains debated. It has been suggested to be the result of the above mentioned isotope-selective photo-dissociation of $N_2$ in the protoplanetary disc but a consensus on the origin of the $^{14}N/^{15}N$ values measured in solar system comets across all molecules is still missing.

Fractionation of carbon isotopes is thought to occur through selective photodissociation of CO and exothermic isotope exchange reactions. Models predict that different levels of fractionation through isotope exchange reaction are expected between molecules formed from CO (like $CO_2$) and molecules formed from $C^+$ (like HCN and CN), with molecules formed from CO richer in $^{13}C$ [24]. However, this has been challenged by measurements of $^{12}C/^{13}C$ in dense clouds, with values either similar to the Interstellar Medium (ISM) or enriched in $^{13}C$ [12]. Measurements of $^{12}C/^{13}C$ isotopes in solar system comets were originally made from observations of $C_2$ and CN, with values around 90, consistent with solar and terrestrial values [17, 18]. In-situ measurements in CO, $CO_2$, $CH_4$, $C_2H_6$ and $CH_3OH$ by the ROSINA mass spectrometer onboard Rosetta at comet 67P revealed similar values in the range 84-91, with only $H_2CO$ showing a lower value of 40 [25–27].

We performed observations of 3I with the UV-Visual Echelle Spectrograph (UVES) on the Very Large Telescope between 6 and 26 December 2025, from which we measure isotopic ratios for $^{14}N/^{15}N$ and $^{12}C/^{13}C$ in CN. Details about the observations and data analysis are presented in the Methods section 1. We measure $^{12}C/^{13}C = 151^{+110}_{-44}$ and $^{14}N/^{15}N = 363^{+633}_{-153}$. The spectra co-added for all dates with lines combined are presented in Fig. 1 for both $^{13}CN$ and $C^{15}N$. The uncertainties given are the 3-sigma uncertainties from the Markov Chain Monte Carlo (MCMC) fit.

The $^{14}N/^{15}N$ ratio in 3I is compared to values measured in solar system comets and other environments in Fig. 2. This is the first measurement of the nitrogen isotopic ratio in an interstellar comet. The $^{14}N/^{15}N$ ratio measured for 3I is significantly larger than the value of $\sim 150$ that is the average measured for solar system comets. It is higher than the ISM value of $274 \pm 18$ [28], but still consistent within the uncertainties, and is close to the solar value of $458.7 \pm 4.2$ [29]. It is consistent with values measured from HCN in pre-stellar cores and proto-stars, which vary between $\sim 150$ and 450 depending on the target [30], as well as with even higher values measured for other species [12]. The $^{14}N/^{15}N$ abundance ratio has been measured in star formation regions

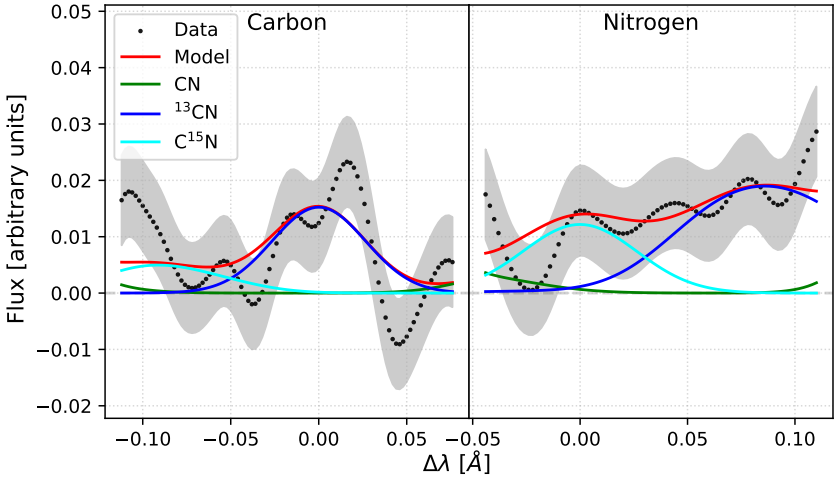


**Fig. 1**: **Co-added observed spectra of 3I with best-fit model** Observed and modelled $^{13}$CN-centred (left) and C$^{15}$N-centred (right) line profiles. The shaded region represents the uncertainty of the profile resulting from the combination of the different lines.

across the Milky Way, with values ranging from $\sim$ 200 to $\sim$ 800. [31] report a trend of slightly increasing $^{14}$N/$^{15}$N ratios until about 11 kpc from the galactic centre, with a decrease after this distance. Given the spread of values even at similar galactocentric distances and their large uncertainties, it is impossible to pinpoint an origin for 3I in a specific region of the galaxy or around a specific type of star from the value of the nitrogen isotopic ratios.

The $^{14}$N/$^{15}$N ratio has been measured in several protoplanetary discs. Disc-integrated measurements of HCN initially revealed a higher abundance of heavy nitrogen compared to pre-stellar cores [12], with values consistent with solar system comets and about a factor two lower than what we measure for 3I. [32] provided the first tentative evidence for increasing $^{14}$N/$^{15}$N ratios with distance from the host star in protoplanetary discs. These measurements were obtained making the hypothesis of a fixed $^{12}$C/$^{13}$C ratio, which is currently under scrutiny and might not be valid. If the $^{12}$C/$^{13}$C ratio varies with the distance in the disc, it would impact the trend of increasing $^{14}$N/$^{15}$N ratios with distance from the host star, making these results harder to interpret. However, later measurements of the T Tauri star TW Hya made without assuming a constant $^{12}$C/$^{13}$C ratio in the protoplanetary disc confirmed the $^{14}$N/$^{15}$N ratios increase with stellar distance in the disc [15]. They measure a disc-average $^{14}$N/$^{15}$N ratio of 223$\pm$21, with values of 121$\pm$11 at 20 au increasing to 339$\pm$28 at 45 au. More recently, [16] reported a ratio increasing from about 100 at 5 au for PDS 70, peaking at more than 300 around 40 au and then decreasing at larger distances from the star (similarly to [15], they did not assume a constant $^{12}$C/$^{13}$C ratio in the protoplanetary disc). These trends have been attributed to shielding in the inner

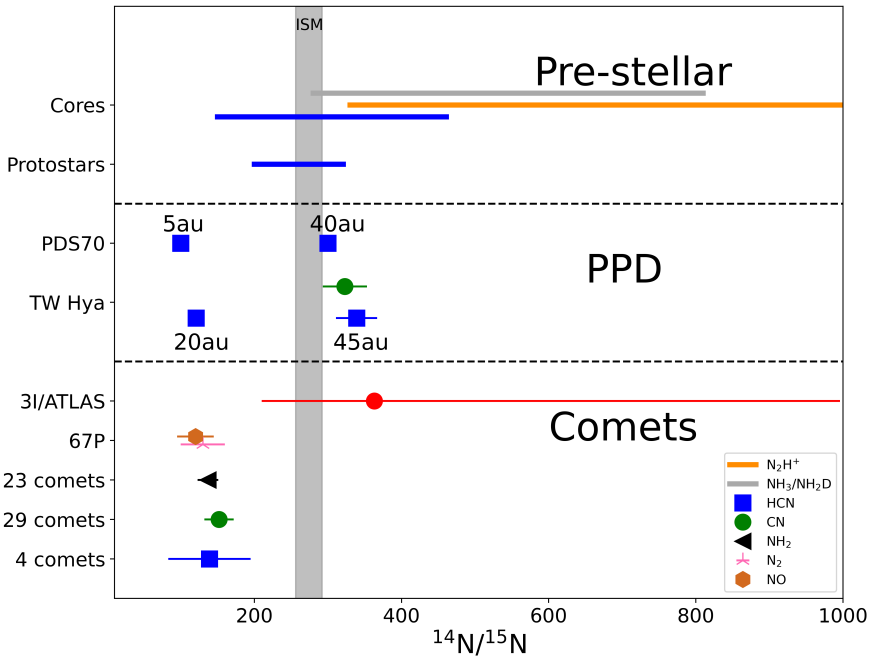


**Fig. 2**: **Comparison of $^{14}N/^{15}N$ in different types of objects** $^{14}N/^{15}N$ isotopic ratios in solar system comets measured from HCN, CN, and $NH_2$ are at the bottom, with different molecules represented by different symbols (values and references are listed in Table 3). 3I is the red circle, with a $^{14}N/^{15}N$ ratio measured in CN and 3-sigma uncertainties. Values for protoplanetary discs, pre-stellar cores, and protostars follow the same convention. Values from protoplanetary discs (PPD) come from [15, 16]. Prestellar $^{14}N/^{15}N$ values come from [30] for HCN and from [12] for the other molecules.

part of protoplanetary discs, making the isotope-selective photo-dissociation of $N_2$ less efficient and preventing enrichment in $^{15}N$. The $^{14}N/^{15}N$ we measure could indicate that 3I was formed in a part of the disc where the isotope-selective photo-dissociation of $N_2$ is not very efficient. This could indicate a formation at a relatively large distance from the star or more generally in an environment where shielding prevents isotope-selective photo-dissociation of $N_2$.

The $^{12}C/^{13}C$ isotope ratio in 3I is significantly higher than the values measured in CN for solar system comets, which average around 90 and range from 65 to ∼100 [18]. This is illustrated in Fig. 3. The value we measure is higher than the current local ISM value of $69 \pm 6$ [33]. $^{12}C/^{13}C$ was constrained for the first time in an interstellar object by [6], who set a lower limit of $^{12}C/^{13}C > 63$ in 3I from the detection of $CO_2$

and $^{13}CO_2$ using NIRSPEC on the JWST. [34] reported a $^{12}C/^{13}C$ in $CO_2$ of $\sim 100$. More recently, [7] report a $^{12}C/^{13}C$ ratio in $CO_2$ and CO in the range 129–196 from JWST observations. This is consistent with our measurement of the same ratio in CN.

**ISOs inherit properties from their parent stars [35]. Modelling by [36] and work by [37] suggests that 3I originated around an old low-metallicity star. Chemical evolution models presented by [41] indicate that high $^{12}C/^{13}C$ ratios are expected around low-metallicity stars. This is supported by observations of a radial gradient in the $^{12}C/^{13}C$ ratio with distance from the galactic centre, with lower values (20-25) towards the centre of the Milky way and larger (up to ∼130) ratios at large galactocentric distances [38, 39], matching the well-known metallicity gradient. This is attributed to the degree of stellar nucleosynthesis in different regions of the galaxy; as the galaxy becomes more chemically complex, more $^{13}C$ is produced relative to $^{12}C$, for example through the CNO cycle in asymptotic giant branch stars [40]. Therefore, the relatively low abundance of $^{13}C$ we measure is consistent with an origin of 3I around a low-metallicity star.**

Processes occurring during the stellar and planetary formation stages could also result in high $^{12}C/^{13}C$ ratios. The $^{12}C/^{13}C$ ratio in 3I is higher than that reported for protoplanetary discs; [15] measure $86 \pm 4$ from HCN in the TW Hya protoplanetary disc and [16] report values $< 100$ for PDS70 at stellar distances smaller than 100 au. Contrary to the nitrogen ratio, there is no strong indication of variation of the carbon isotopic ratio within discs, except potentially for PDS70 at large distances from the star [16]. Models predict that the dominant mechanism for carbon isotope fractionation in discs is the exothermic exchange reaction:

$$CO + {}^{13}C^{+} \rightleftharpoons {}^{13}CO + C^{+} + 35\,K$$

In that scenario, molecules formed from $C^+$ (like CN) are $^{13}$C-poor, while molecules formed from CO are $^{13}$C-rich. As demonstrated in [12], scenarios where the absorption is low, leading to sufficient far-ultra-violet radiation, can result in high $^{12}C/^{13}C$ in HCN. This would be consistent with 3I forming in the outer disc, where photons can scatter and reach deeper layers. Recent work by [42] also investigated the effect of the carbon to oxygen elemental ratio in protoplanetary discs. Their model indicates that an abundance ratio of $C/O \sim 1-1.5$ (higher than the C/O in solar twins $\sim$ 0.5 or the Sun $\sim$ 0.55 [43, 44]) can result in $H^{12}CN/H^{13}CN$ ratios larger than 100. This could be consistent with the large abundance of CO and $CO_2$ relative to water reported by [6, 7].

Scenarios involving exothermic exchange reactions in the protoplanetary disc as mentioned in the previous paragraph are expected to lead to two different reservoirs. On one side, molecules formed from $C^+$ (like CN) would have a high $^{12}C/^{13}C$ ratio and on the other side, molecules forming from CO would have a lower ratio. As $^{13}$C is exchanged between the two reservoirs depending on the conditions, if the starting $^{12}C/^{13}C$ ratio is similar to the solar system, a much higher $^{12}C/^{13}C$ for CN should be coupled to a lower ratio in CO and $CO_2$. **Differences between carbon isotopic ratios measured in $C_2H$ and CO have been reported in the TW Hya protoplanetary disk [85].** However, this is not consistent with measurement of the

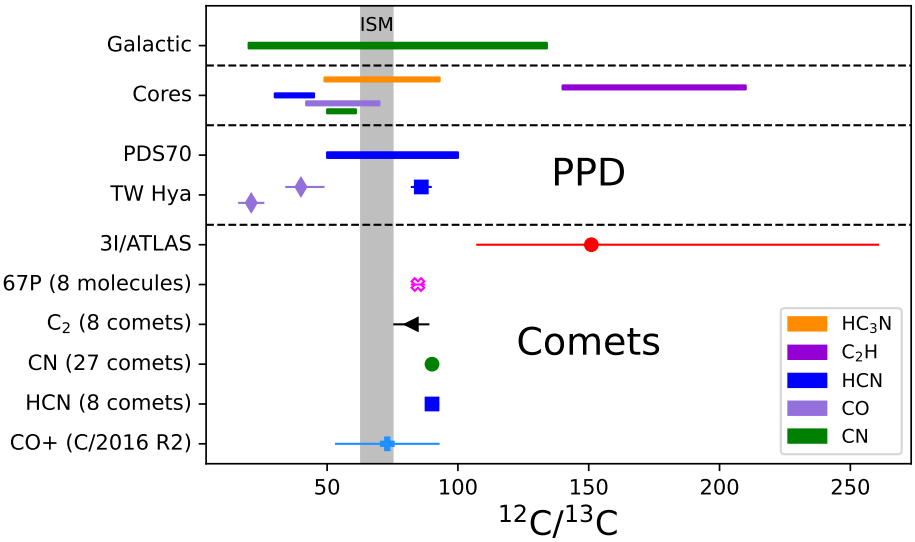


**Fig. 3**: **Comparison of $^{12}C/^{13}C$ in different types of objects** $^{12}C/^{13}C$ isotopic ratios in solar system comets were measured from various molecules, with different molecules represented by different symbols. Plotted values are the weighted average and uncertainty of all published values listed in Table 4; in some cases multiple measurements were included for a single comet. The 67P point represents the weighted average of nine measurements of eight molecules obtained in situ during the Rosetta mission. 3I is the red circle with 3-sigma uncertainties. Values for protoplanetary discs [15, 16, 45, 46], pre-stellar cores [12], galactic [39], and ISM [33] follow the same color convention and are identified in the legend.

$^{12}C/^{13}C$ ratio in CO and $CO_2$ in 3I by JWST which is similarly high to what we measure in CN. Both measurements have relatively large uncertainties but are significantly higher than solar system-like ratios. **The high $^{12}C/^{13}C$ in CN, CO, and $CO_2$ for 3I thus favours an origin from a $^{13}C$-poor reservoir. The combination of JWST and VLT measurements indicates that the high $^{12}C/^{13}C$ in 3I/ATLAS is more compatible with formation around an older low-metallicity star rather than processes in the protoplanetary disc.**

Work by [47] indicated that the long residence of 3I in interstellar space (on the order of ∼Gyrs) likely resulted in galactic cosmic ray processing of the surface layers of 3I, which could have affected the composition of the gas observed, particularly pre-perihelion. Our observations were all performed post-perihelion, at a time when the comet had been very active for several months. Integrating the water production rate over the perihelion passage, and assuming a gas-to-dust ratio of unity, we estimate that the comet lost a surface layer of at least 5 m, if the mass loss was distributed uniformly across the nucleus (Xing et al in prep). This estimate adopts a nucleus radius of $1.3 \pm 0.2$ km [48]. **Given the material loss experienced by 3I about perihelion, the gas in the coma probed by this work could originate from**

**deeper layers that were possibly unaffected by processing, even though it is difficult to confirm given the currently available measurements.**

In summary, using observations of the CN molecule with the UVES spectrograph at the VLT, we measure a high $^{14}N/^{15}N$ isotopic ratio in the interstellar comet 3I, a factor of two higher than what is measured in solar system comets but consistent with measurements of the same ratio in CN or HCN in pre-stellar cores, protostars, and at larger stellar distances in protoplanetary discs. We measure a $^{12}C/^{13}C$ ratio higher than that of solar system comets. This is compatible with values expected for older, low-metallicity stars.

# 1 Methods

## 1.1 Observations

Observations were performed with the UV-Visual Echelle Spectrograph (UVES[2]) at the European Southern Observatory (ESO) Very Large Telescope (VLT) Unit Telescope 2 (UT2), under programme 115.28NL.003. Observations were obtained as soon as possible after perihelion, over a period ranging from 6 to 26 December 2025. While observations with UVES as part of this programme span a longer period of time, we selected observations with the highest signal to noise ratio for this work. We used two different settings to cover the entire optical range: 348+580 (dichroic 1) covering the ranges 3050-3888 Å in the blue and 4760-6840 Å in the red, and 437+860 (dichroic 2) covering the range 3740-4990 Å in the blue and 6600-10600 Å in the red. The slit width was set to 0.6", providing a resolving power of ∼60,000. In this manuscript, we will focus on observations with the blue arm of each setting as they contain the CN $B^2\Sigma^+$-$X^2\Sigma^+$ (0,0) emission band which we are interested in (around 3880 Å). The observational circumstances of the spectra used in this work are presented in Table 1.

**Table 1**: Observational circumstances. $r_h$ is the heliocentric distance, $\dot{r_h}$ the heliocentric velocity, $\Delta$ the geocentric distance, and $\dot{\Delta}$ the geocentric velocity.

| Date (UT) | Set-up | $r_h$ | $\dot{r_h}$ | $\Delta$ | $\dot{\Delta}$ | Exp. Time |
|---|---|---|---|---|---|---|
| DD-MM-YYYY HH:MM-HH:MM | | au | km/s | au | km/s | # × s |
| 06-12-2025 07:25-08:25 | 348+580 | 1.93 | 44.5 | 1.86 | -15.5 | 3×1000 |
| 10-12-2025 07:10-08:35 | 437+860 | 2.04 | 46.5 | 1.83 | -11.6 | 3×1600 |
| 15-12-2025 07:05-07:56 | 348+580 | 2.18 | 48.6 | 1.80 | -5.8 | 3×1300 |
| 21-12-2025 05:40-07:35 | 348+580 | 2.35 | 50.6 | 1.80 | 2.8 | 2×3400 |
| 21-12-2025 07:40-08:35 | 437+860 | 2.35 | 50.6 | 1.80 | 3.1 | 1×3400 |
| 26-12-2025 07:05-07:55 | 348+580 | 2.50 | 51.9 | 1.82 | 11.3 | 1×3200 |

[2]UVES User Manual, VLT-MAN-ESO-13200-1825,
https://www.eso.org/sci/facilities/paranal/instruments/instruments.html

## 1.2 Data reduction

Before processing with the ESO pipeline, cosmic ray hits were removed from the raw frames using the "lacosmic" package [50]. The data were then reduced using the ESO UVES pipeline, resulting in flux and wavelength-calibrated 2D spectra. The spectrum extraction (over the full slit length) and subtraction of the continuum were performed using custom python scripts following the procedure described in [17], resulting in wavelength and flux-calibrated 1D spectra. The wavelength calibration was refined using CN and solar lines, yielding an accuracy better than 0.1 km/s. Particular care was taken to remove solar light scattered by cometary dust and by the Earth's atmosphere (twilight and moonlight).

## 1.3 Modelling and data fitting

Fluorescence models of the three isotopologues ($^{12}C^{14}N$, $^{13}C^{14}N$, $^{12}C^{15}N$) were computed for each spectrum using the model described in [17]. The instrumental line profile was adjusted to the observations through a convolution kernel computed with the IRAF $psfmatch$ procedure. The observed spectra and the models were then optimally combined according to their signal-to-noise ratios. Isotopic lines were not individually detected, even in a co-added spectrum containing all dates. As a result, we co-added a selection of lines into a single profile to enable the detection of the isotopes' signatures, as has been done in previous work to detect faint isotopic signature [51, 52]. We carefully selected lines to avoid contamination by any known cometary or telluric emission line and provide the cleanest combined profile possible. Combinations of lines were done separately to produce a final observed spectrum centred for $^{13}C^{14}N$ and $^{12}C^{15}N$ respectively. This resulted in a total of five co-added lines for $^{13}C^{14}N$ and 10 lines for $^{12}C^{15}N$. The selected lines are listed in Table 2 and the resulting profiles are displayed in Figure 1. Both profiles show a peak centred at 0 due to $^{13}C^{14}N$ and $^{12}C^{15}N$ respectively, with the $^{12}C^{15}N$ profile showing an additional region of higher flux around 0.08 due to the signature of $^{12}C^{14}N$. In addition to these, wiggles can be seen in the combined profiles, resulting from the co-addition of low signal-to-noise ratios spectra and lines to create the profiles.

Isotopic abundances were derived from the combined profiles of selected lines for each isotopologue. A linear combination of CN, $^{13}CN$ and $C^{15}N$ was fitted for both of the $^{13}CN$-centred and $C^{15}N$-centred profiles. Despite a careful continuum correction, the final profiles were seen to have an offset from the zero level. This is the result of large-scale wiggles in the spectrum introduced by the flux calibration process, which is a documented effect for the UVES instrument. We tried different fitting methods to account for this, which all gave similar results. First, we minimized the standard deviation of the residuals between the model and the observations for the carbon- and nitrogen-centred profiles simultaneously. This technique is insensitive to a constant offset in the underlying background and thus provides a reliable way to estimate the isotopic ratios in this case. Isotopic ratio uncertainties were estimated using a jackknife resampling technique that successively removed one of the lines from the line co-addition. This method for estimating uncertainties is particularly sensitive to potential unidentified lines in the selected ranges or local over/under-subtraction of

**Table 2**: Lines used to produce combined profiles for $^{13}$CN and C$^{15}$N

| Wavelength Å | Species | Weight |
|---|---|---|
| 3864.877 | $^{13}$CN | 3.4016 |
| 3866.374 | C$^{15}$N | 13.7924 |
| 3867.172 | C$^{15}$N | 17.8456 |
| 3867.955 | C$^{15}$N | 20.4280 |
| 3869.464 | C$^{15}$N | 36.6548 |
| 3869.567 | $^{13}$CN | 39.4362 |
| 3870.189 | C$^{15}$N | 23.2371 |
| 3870.285 | $^{13}$CN | 31.1156 |
| 3870.894 | C$^{15}$N | 17.6514 |
| 3871.581 | C$^{15}$N | 21.1103 |
| 3871.660 | $^{13}$CN | 18.9411 |
| 3872.249 | C$^{15}$N | 31.3997 |
| 3873.526 | C$^{15}$N | 23.9557 |
| 3873.582 | $^{13}$CN | 23.8820 |
| 3874.135 | C$^{15}$N | 21.9128 |

the continuum and presents a way to estimate the impact of systematics on the results. With this technique, we measure $^{12}$C/$^{13}$C $= 147^{+87}_{-40}$ and $^{14}$N/$^{15}$N $= 343^{+454}_{-124}$. The jackknife technique is illustrated in Figure 4, where we display three sets of profiles where a line was removed. In each case, the final shape of the profile is similar to the profile with all lines co-added presented in Figure 1. However, the jackknife variance tends to be overestimated for small sample sizes, which is our case with 5 and 10 lines.

To get a better quantification of the uncertainties of our measurements, we also fitted the profiles (with the full set of lines) using the python MCMC *emcee* package. For those fits, the value of the background level matters, so we included offsets for the $^{13}$CN-centred and C$^{15}$N-centred profiles, respectively, in addition to the values of the isotopic ratios, as free parameters. We used loose boundary conditions for all fitted parameter but introduced a more informed prior for the $^{14}$N/$^{15}$N ratio to ensure physically meaningful results, with the ratio set to be between 0 and 1000, encompassing the range of values measured in pre-stellar cores. The MCMC fit resulted in $^{12}$C/$^{13}$C $= 151^{+110}_{-44}$ and $^{14}$N/$^{15}$N $= 363^{+633}_{-153}$, with the uncertainties stated at the 3-sigma level. The corner plot with the MCMC a posteriori distribution of our fitted parameters (including the offsets) is shown in Figure 5. The values given here for the ratios are the mode of the posterior distributions, which are the most likely value of the parameter. For $^{14}$N/$^{15}$N, the posteriori distribution is asymmetrical and the mode and median of the distribution differ significantly, as illustrated in Figure 5. For comparison, the medians of the posterior distributions are: $^{12}$C/$^{13}$C $= 159$ and $^{14}$N/$^{15}$N $= 458$. The offset parameters are 0.0124 and 0.0260 (in arbitrary flux units) for the $^{13}$CN-centred and C$^{15}$N-centred profiles, respectively. The results from both techniques (jackknife and MCMC) agree very well within the uncertainties and we have adopted the MCMC mode values and 3-sigma uncertainties in the rest of the manuscript.

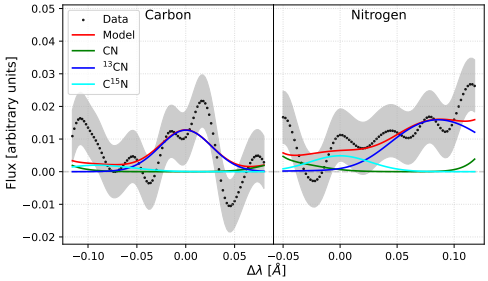


(a) The $^{13}$CN 3864.877 Å line was removed. The measured isotopic ratios for this profile are: $^{12}$C/$^{13}$C = 192 and $^{14}$N/$^{15}$N = 935.

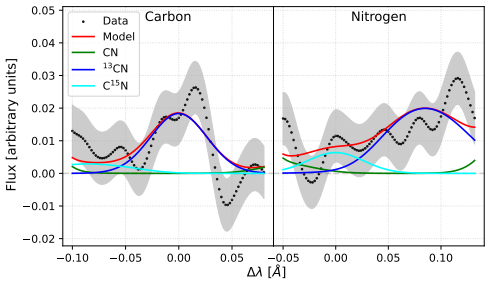


(b) **The C$^{15}$N 3866.374 Å line was removed.** The measured isotopic ratios for this profile are: $^{12}$C/$^{13}$C = 152 and $^{14}$N/$^{15}$N = 688.

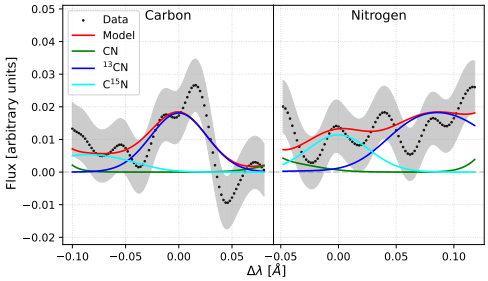


(c) **The C$^{15}$N 3870.894 Å line was removed**. The measured isotopic ratios for this profile are: $^{12}$C/$^{13}$C = 154 and $^{14}$N/$^{15}$N = 371.

**Fig. 4**: **Co-added observed spectra of 3I with best-fit model.** Observed (dotted line) and modelled (solid lines) $^{13}$CN-centred (left) and C$^{15}$N-centred (right) line profiles. The shaded region represents the uncertainty of the profile resulting from the combination of the different lines, estimated from the jackknife technique removing a single line for each panel.

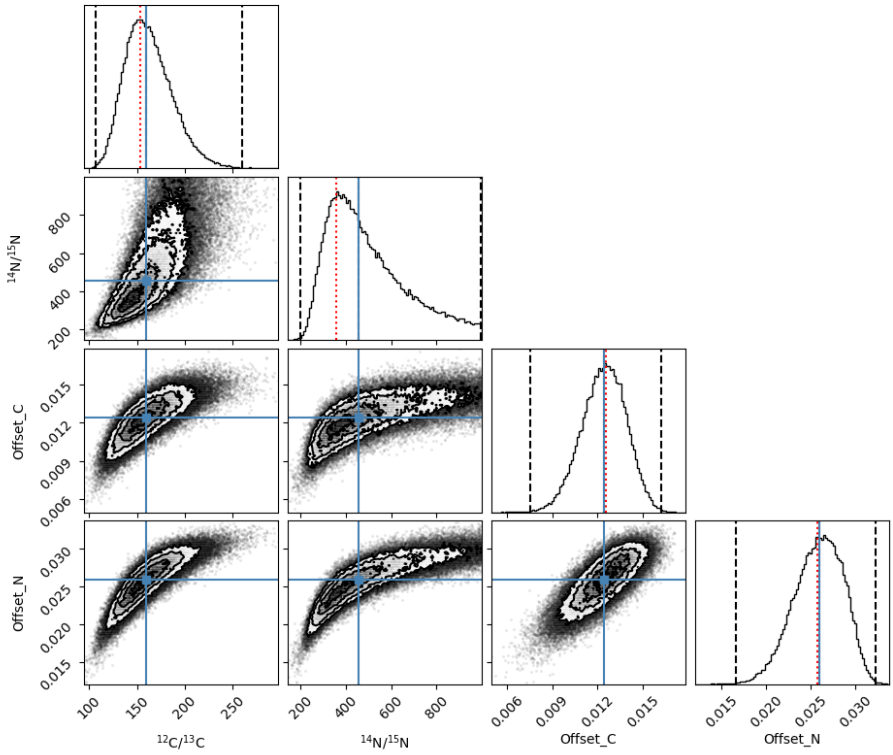


**Fig. 5**: **MCMC a posteriori distributions for the fitted parameters** The solid blue, red dotted, and black dashed lines show the median, mode, and 3-sigma boundaries of the distributions, respectively.

**Table 3**: Nitrogen isotope ratios plotted in Figure 2.

| **Species** | **Comet** | $^{14}N/^{15}N$ | **Reference** |
|---|---|---|---|
| HCN | C/1995 O1 (Hale-Bopp) | 205 ± 70 | [53] |
| | C/2014 Q2 (Lovejoy) | 145 ± 12 | [54] |
| | 17P/Holmes | 139 ± 26 | [54] |
| | 46P/Wirtanen | 68 ± 27 | [20] |
| CN | C/1995 O1 (Hale-Bopp) | 130 ± 40 | [55], revised in [17] |
| | | 150 ± 30 | [55], revised in [17] |
| | | 135 ± 40 | [55], revised in [17] |
| | C/1999 S4 (LINEAR) | 150 ± 40 | [56], revised in [17] |
| | C/2000 WM1 (LINEAR) | 150 ± 30 | [57], revised in [17] |
| | C/2001 Q4 (NEAT) | 130 ± 40 | [55] |
| | C/2002 T7 (LINEAR) | 160 ± 25 | [17] |
| | C/2002 V1 (NEAT) | 160 ± 35 | [17] |
| | C/2002 X5 (Kudo-Fujikawa) | 130 ± 20 | [17] |
| | C/2002 Y1 (Juels-Holvorcem) | 150 ± 35 | [17] |
| | C/2003 K4 (LINEAR) | 150 ± 35 | [55], revised in [17] |
| | | 145 ± 25 | [55], revised in [17] |
| | C/2006 M4 (SWAN) | 145 ± 50 | [17] |
| | C/2007 N3 (Lulin) | 150 ± 50 | [17] |
| | C/2015 ER61 (PanSTARRS) | 130 ± 15 | [58] |
| | 8P/Tuttle | 150 ± 30 | [59] |
| | 9P/Tempel 1 | 110 ± 20 | [60] |
| | | 45 ± 20 | [60] |
| | 17P/Holmes | 165 ± 35 | [53] |
| | | 150 ± 50 | [17] |
| | 21P/Giacobini-Zinner | 145 ± 10 | [61] |
| | 46P/Wirtanen | 150 ± 30 | [21] |
| | 73P-B/Schwassmann-Wachmann 3 | 210 ± 50 | [62] |
| | 73P-C/Schwassmann-Wachmann 3 | 220 ± 40 | [62] |
| | 88P/Howell | 140 ± 20 | [56] |
| | 103P/Hartley 2 | 155 ± 25 | [63] |
| | 122P/de Vico | 145 ± 20 | [64] |
| | 153P/Ikeya-Zhang | 140 ± 50 | [64] |
| | 3I/ATLAS | $363^{+633}_{-153}$ | this work |
| $NH_2$ | C/2000 WM1 (LINEAR) | 132 ± 31 | [65] |
| | C/2001 Q4 (NEAT) | 145 ± 35 | [65] |
| | | 126 ± 30 | [65] |
| | C/2002 T7 (LINEAR) | 138 ± 25 | [65] |
| | C/2002 V1 (NEAT) | 132 ± 32 | [65] |
| | C/2002 X5 (Kudo-Fujikawa) | 137 ± 27 | [65] |
| | C/2002 Y1 (Juels Holvorcem) | 132 ± 33 | [65] |
| | C/2003 K4 (LINEAR) | 153 ± 63 | [65] |
| | C/2009 P1 (Garradd) | 154 ± 41 | [65] |
| | | 132 ± 61 | [65] |

| Species | Comet | $^{14}N/^{15}N$ | Reference |
|---|---|---|---|
| | C/2012 F6 (Lemmon) | 155 ± 28 | [65] |
| | | 152 ± 72 | [54] |
| | C/2012 S1 (ISON) | 139 ± 38 | [66] |
| | C/2013 R1 (Lovejoy) | 126 ± 28 | [65] |
| | | 100 ± 50 | [67] |
| | C/2013 US10 (Catalina) | 149 ± 32 | [65] |
| | C/2014 E2 (Jacques) | 126 ± 55 | [65] |
| | C/2014 Q2 (Lovejoy) | 126 ± 25 | [68] |
| | | 145 ± 12 | [54] |
| | C/2015 ER61 (PanSTARRS) | 140 ± 28 | [58] |

**Table 4**: Carbon isotope ratios plotted in Figure 3.

| Species | Comet | $^{12}C/^{13}C$ | Reference |
|---|---|---|---|
| $C_2$ | C/1963 A1 (Ikeya) | 70 ± 15 | [69] |
| | C/1969 T1 (Tago-Sato-Kosaka) | 100 ± 20 | [70] |
| | C/1973 E1 (Kohoutek) | $115^{+30}_{-20}$ | [71] |
| | | $135^{+65}_{-45}$ | [71] |
| | C/1975 N1 (Kobayashi-Berger-Milon) | $100^{+20}_{-30}$ | [72] as reported in [73] |
| | C/1975 V1 (West) | 60 ± 15 | [74] |
| | C/2001 Q4 (NEAT) | 80 ± 20 | [67] |
| | C/2002 T7 (LINEAR) | 85 ± 20 | [67] |
| | C/2012 S1 (ISON) | 94 ± 33 | [66] as reported in [18] |
| CN | C/1989 Q1 (Okazaki-Levy-Rudenko) | 93 ± 20 | [73] |
| | C/1989 X1 (Austin) | 85 ± 20 | [73] |
| | C/1990 K1 (Levy) | 90 ± 10 | [73] |
| | C/1995 O1 (Hale-Bopp) | 90 ± 15 | [75] |
| | | 90 ± 20 | [55], revised in [17] |
| | | 100 ± 30 | [55], revised in [17] |
| | | 80 ± 25 | [55], revised in [17] |
| | C/1999 S4 (LINEAR) | 90 ± 30 | [56], revised in [17] |
| | C/2000 WM1 (LINEAR) | 100 ± 20 | [57], revised in [17] |
| | C/2001 Q4 (NEAT) | 90 ± 15 | [55] |
| | | 70 ± 30 | [55] |
| | C/2002 T7 (LINEAR) | 85 ± 20 | [17] |
| | C/2002 V1 (NEAT) | 100 ± 20 | [17] |
| | C/2002 X5 (Kudo-Fujikawa) | 90 ± 20 | [17] |
| | C/2002 Y1 (Juels-Holvorcem) | 90 ± 20 | [17] |
| | C/2003 K4 (LINEAR) | 90 ± 20 | [55], revised in [17] |
| | | 80 ± 20 | [55], revised in [17] |
| | C/2006 M4 (SWAN) | 95 ± 25 | [17] |
| | C/2007 N3 (Lulin) | 105 ± 40 | [17] |
| | C/2012 F6 (Lemmon) | 95 ± 25 | [18] |
| | C/2015 ER61 (PanSTARRS) | 100 ± 15 | [58] |
| | 1P/Halley | 65 ± 9 | [76] |
| | | 89 ± 17 | [77] |
| | | 95 ± 12 | [78] |
| | 8P/Tuttle | 90 ± 20 | [59] |
| | 9P/Tempel 1 | 95 ± 15 | [60] |
| | | 110 ± 20 | [60] as reported in [17] |
| | 17P/Holmes | 90 ± 20 | [53] |
| | | 90 ± 20 | [17] |
| | 21P/Giacobini-Zinner | 100 ± 10 | [61] |
| | 46P/Wirtanen | 100 ± 20 | [21] |
| | 73P-B/Schwassmann-Wachmann 3 | 100 ± 30 | [62] |
| | 73P-C/Schwassmann-Wachmann 3 | 100 ± 20 | [62] |
| | 88P/Howell | 90 ± 10 | [56] |

| **Species** | **Comet** | $^{12}C/^{13}C$ | **Reference** |
|---|---|---|---|
| | 103P/Hartley 2 | 95 ± 15 | [63] |
| | 122P/de Vico | 90 ± 10 | [64] |
| | 153P/Ikeya-Zhang | 80 ± 30 | [64] |
| | 3I/ATLAS | $151^{+110}_{-44}$ | this work |
| HCN | C/1995 O1 (Hale-Bopp) | 111 ± 12 | [79] |
| | | 94 ± 8 | [53] |
| | | 109 ± 22 | [80] |
| | C/1996 B2 (Hyakutake) | 34 ± 12 | [81] |
| | C/2012 F6 (Lemmon) | 124 ± 64 | [54] |
| | C/2012 S1 (ISON) | 88 ± 18 | [82] |
| | C/2014 Q2 (Lovejoy) | 109 ± 14 | [54] |
| | C/2022 E3 (ZTF) | 135 ± 75 | [18] |
| | 17P/Holmes | 114 ± 26 | [53] |
| | 46P/Wirtanen | 90 ± 28 | [20] |
| CO+ | C/2016 R2 (PanSTARRS) | 73 ± 20 | [83] |
| CO | 67P/Churyumov-Gerasimenko | 86 ± 9 | [25] |
| $CO_2$ | 67P/Churyumov-Gerasimenko | 84 ± 4 | [26] |
| $CH_4$ | 67P/Churyumov-Gerasimenko | 88 ± 10 | [84] |
| $C_2H_6$ | 67P/Churyumov-Gerasimenko | 93 ± 10 | [84] |
| | | 105 ± 10 | [27] |
| $C_3H_8$ | 67P/Churyumov-Gerasimenko | 87 ± 9 | [84] |
| $C_4H_{10}$ | 67P/Churyumov-Gerasimenko | 96 ± 14 | [84] |
| $H_2CO$ | 67P/Churyumov-Gerasimenko | 40 ± 14 | [27] |
| $CH_3OH$ | 67P/Churyumov-Gerasimenko | 91 ± 10 | [27] |

## Acknowledgements

The authors wish to acknowledge the exceptional level of support provided by support astronomers, Telescope and Instrument Operators, and User Support Department at Paranal Observatory. **We thank Matthew Hopkins for useful discussions on the galactic origins of ISOs.** CO acknowledges the support of the Royal Society under grant URF\R1\211429. MAC was supported by NASA's Planetary Science Division Internal Scientist Funding Program through the Fundamental Laboratory Research work package (FLaRe). The views expressed in this article are those of the authors and do not reflect the official policy or position of the U.S. Naval Academy, Department of the Navy, the Department of Defense, or the U.S. Government. RCD acknowledges support from grant #361233 awarded by the Research Council of Finland to M. Granvik. JM is honorary Research Director at the F.R.S-FNRS. DH and EJ are Research Directors at the F.R.S.-FNRS. M.T.B. appreciates support by the Rutherford Discovery Fellowships from New Zealand Government funding, administered by the Royal Society Te Apārangi. For the purpose of open access, the authors have applied a Creative Commons Attribution (CC BY) licence to any Author Accepted Manuscript version arising from this submission.

## Data availability

All data used for this work will be available on the European Southern Observatory archive after a proprietary period of one year from the time of observations. They can be accessed searching for the programme number of the observations: 15.28NL.003.

## Author contribution

CO led the data acquisition and the writing of the manuscript. DH led the data reduction. JM led the data analysis. MMK and FL contributed figures and participated to the discussion of the results. EJ, KA, DB, VVG, MC, RCD, LFF, ML, BPM, MTB and SC contributed to the manuscript and discussion of the results.

## References

[1] Williams, G. V. *et al.* Comet C/2017 u1 (panstarrs). *Minor Planet Electronic Circulars* **2017-U181** (2017).

[2] Denneau, L. *et al.* 3I/ATLAS = C/2025 n1 (atlas). *Minor Planet Electronic Circulars* **2025-N12** (2025).

[3] Jewitt, D., Hui, M.-T., Mutchler, M., Kim, Y. & Agarwal, J. Hubble Space Telescope Observations of the Interstellar Interloper 3I/ATLAS. *Astrophys. J.* **990**, L2 (2025).

[4] Alarcon, M. R. *et al.* Deep g'-band Imaging of Interstellar Comet 3I/ATLAS from the Two-meter Twin Telescope (TTT). *The Astronomer's Telegram* **17264**, 1 (2025).

[5] Seligman, D. Z. *et al.* Discovery and Preliminary Characterization of a Third Interstellar Object: 3I/ATLAS. *Astrophys. J.* **989**, L36 (2025).

[6] Cordiner, M. A. *et al.* JWST Detection of a Carbon-dioxide-dominated Gas Coma Surrounding Interstellar Object 3I/ATLAS. *Astrophys. J.* **991**, L43 (2025).

[7] Cordiner, M. *et al.* Isotopic Evidence for a Cold and Distant Origin of the Interstellar Object 3I/ATLAS. *arXiv e-prints* arXiv:2603.06911 (2026).

[8] Harrington Pinto, O., Womack, M., Fernandez, Y. & Bauer, J. A Survey of CO, $CO_2$, and $H_2O$ in Comets and Centaurs. *Planet. Sci. J.* **3**, 247 (2022).

[9] Rahatgaonkar, R. *et al.* VLT observations of interstellar comet 3I/ATLAS II. From quiescence to glow: Dramatic rise of Ni I emission and incipient CN outgassing at large heliocentric distances. *arXiv e-prints* arXiv:2508.18382 (2025).

[10] Hutsemékers, D. *et al.* Pre-perihelion evolution of the NiI/FeI abundance ratio in the coma of the interstellar comet 3I/ATLAS: From extreme to normal. *Astron. Astrophys.* **706**, A43 (2026).

[11] Roth, N. X. *et al.* $CH_3OH$ and HCN in Interstellar Comet 3I/ATLAS Mapped with the ALMA Atacama Compact Array: Distinct Outgassing Behaviors and a Remarkably High $CH_3OH$/HCN Production Rate Ratio. *arXiv e-prints* arXiv:2511.20845 (2025).

[12] Nomura, H. *et al.* Inutsuka, S., Aikawa, Y., Muto, T., Tomida, K. & Tamura, M. (eds) *The Isotopic Links from Planet Forming Regions to the Solar System.* (eds Inutsuka, S., Aikawa, Y., Muto, T., Tomida, K. & Tamura, M.) *Protostars and Planets VII*, Vol. 534 of *Astronomical Society of the Pacific Conference Series*, 1075 (2023).

[13] Wirström, E. S., Charnley, S. B., Cordiner, M. A. & Milam, S. N. Isotopic Anomalies in Primitive Solar System Matter: Spin-state-dependent Fractionation of Nitrogen and Deuterium in Interstellar Clouds. *Astrophys. J.* **757**, L11 (2012).

[14] Wirström, E. S. & Charnley, S. B. Revised models of interstellar nitrogen isotopic fractionation. *Mon. Not. R. Astron. Soc.* **474**, 3720–3726 (2018).

[15] Hily-Blant, P., Magalhaes de Souza, V., Kastner, J. & Forveille, T. Multiple nitrogen reservoirs in a protoplanetary disk at the epoch of comet and giant planet formation. *Astron. Astrophys.* **632**, L12 (2019).

[16] Rampinelli, L. *et al.* Radial variations in the nitrogen, carbon, and hydrogen

fractionation in the PDS 70 planet-hosting disk. *Astron. Astrophys.* **698**, A115 (2025).

[17] Manfroid, J. *et al.* The CN isotopic ratios in comets. *Astron. Astrophys.* **503**, 613–624 (2009).

[18] Biver, N., Dello Russo, N., Opitom, C. & Rubin, M. in *Chemistry of Comet Atmospheres* (eds Meech, K. J., Combi, M. R., Bockelée-Morvan, D., Raymond, S. N. & Zolensky, M. E.) *Comets III* 459–498 (2024).

[19] Altwegg, K., Balsiger, H. & Fuselier, S. A. Cometary Chemistry and the Origin of Icy Solar System Bodies: The View After Rosetta. *ARA&A* **57**, 113–155 (2019).

[20] Cordiner, M. A. *et al.* Evidence for Surprising Heavy Nitrogen Isotopic Enrichment in Comet 46P/Wirtanen's Hydrogen Cyanide. *Planet. Sci. J.* **5**, 221 (2024).

[21] Moulane, Y. *et al.* Activity and composition of the hyperactive comet 46P/Wirtanen during its close approach in 2018. *Astron. Astrophys.* **670**, A159 (2023).

[22] Fray, N., Bénilan, Y., Cottin, H., Gazeau, M.-C. & Crovisier, J. The origin of the CN radical in comets: A review from observations and models. *Planet. Space Sci.* **53**, 1243–1262 (2005).

[23] Sipilä, O. *et al.* Combined model for $^{15}$N, $^{13}$C, and spin-state chemistry in molecular clouds. *Astron. Astrophys.* **678**, A120 (2023).

[24] Langer, W. D., Graedel, T. E., Frerking, M. A. & Armentrout, P. B. Carbon and oxygen isotope fractionation in dense interstellar clouds. *Astrophys. J.* **277**, 581–604 (1984).

[25] Rubin, M. *et al.* Evidence for depletion of heavy silicon isotopes at comet 67P/Churyumov-Gerasimenko. *Astron. Astrophys.* **601**, A123 (2017).

[26] Hässig, M. *et al.* Isotopic composition of $CO_2$ in the coma of 67P/Churyumov-Gerasimenko measured with ROSINA/DFMS. *Astron. Astrophys.* **605**, A50 (2017).

[27] Altwegg, K. *et al.* Molecule-dependent oxygen isotopic ratios in the coma of comet 67P/Churyumov-Gerasimenko. *Mon. Not. R. Astron. Soc.* **498**, 5855–5862 (2020).

[28] Ritchey, A. M., Federman, S. R. & Lambert, D. L. The $C^{14}N/C^{15}N$ Ratio in Diffuse Molecular Clouds. *Astrophys. J.* **804**, L3 (2015).

[29] Marty, B., Chaussidon, M., Wiens, R. C., Jurewicz, A. J. G. & Burnett, D. S. A $^{15}$N-Poor Isotopic Composition for the Solar System As Shown by Genesis Solar Wind Samples. *Science* **332**, 1533 (2011).

[30] Jensen, S. S. *et al.* Fractionation in young cores: Direct determinations of nitrogen and carbon fractionation in HCN. *Astron. Astrophys.* **685**, A149 (2024).

[31] Colzi, L. *et al.* CHEMOUT: CHEMical complexity in star-forming regions of the OUTer Galaxy. III. Nitrogen isotopic ratios in the outer Galaxy. *Astron. Astrophys.* **667**, A151 (2022).

[32] Guzmán, V. V., Öberg, K. I., Huang, J., Loomis, R. & Qi, C. Nitrogen Fractionation in Protoplanetary Disks from the $H^{13}CN/HC^{15}N$ Ratio. *Astrophys. J.* **836**, 30 (2017).

[33] Wilson, T. L. Isotopes in the interstellar medium and circumstellar envelopes. *Reports on Progress in Physics* **62**, 143–185 (1999).

[34] Lisse, C. M. *et al.* SPHEREx Discovery of Strong Water Ice Absorption and an Extended Carbon Dioxide Coma in 3I/ATLAS. *Research Notes of the American Astronomical Society* **9**, 242 (2025).

[35] Hopkins, M. J. *et al.* The Galactic Interstellar Object Population: A Framework for Prediction and Inference. *Astron. J.* **166**, 241 (2023).

[36] Hopkins, M. J. *et al.* From a Different Star: 3I/ATLAS in the Context of the Ōtautahi–Oxford Interstellar Object Population Model. *Astrophys. J.* **990**, L30 (2025).

[37] Taylor, A. G. & Seligman, D. Z. The Kinematic Age of 3I/ATLAS and Its Implications for Early Planet Formation. *Astrophys. J.* **990**, L14 (2025).

[38] Yan, Y. T. *et al.* Direct measurements of carbon and sulfur isotope ratios in the Milky Way. *Astron. Astrophys.* **670**, A98 (2023).

[39] Milam, S. N., Savage, C., Brewster, M. A., Ziurys, L. M. & Wyckoff, S. The $^{12}C/^{13}C$ Isotope Gradient Derived from Millimeter Transitions of CN: The Case for Galactic Chemical Evolution. *Astrophys. J.* **634**, 1126–1132 (2005).

[40] Timmes, F. X., Woosley, S. E. & Weaver, T. A. Busso, M., Raiteri, C. M. & Gallino, R. (eds) *Galactic Chemical Evolution: Neutrino-Process Contributions.* (eds Busso, M., Raiteri, C. M. & Gallino, R.) *Nuclei in the Cosmos III*, Vol. 327 of *American Institute of Physics Conference Series*, 543 (AIP, 1995).

[41] Kobayashi, C., Karakas, A. I. & Umeda, H. The evolution of isotope ratios in the Milky Way Galaxy. *Mon. Not. R. Astron. Soc.* **414**, 3231–3250 (2011).

[42] Lee, S., Nomura, H. & Furuya, K. Carbon Isotope Chemistry in Protoplanetary Disks: Effects of C/O Ratios. *Astrophys. J.* **969**, 41 (2024).

[43] Bedell, M. *et al.* The Chemical Homogeneity of Sun-like Stars in the Solar Neighborhood. *Astrophys. J.* **865**, 68 (2018).

[44] Nissen, P. E. High-precision abundances of elements in solar twin stars. Trends with stellar age and elemental condensation temperature. *Astron. Astrophys.* **579**, A52 (2015).

[45] Zhang, K., Bergin, E. A., Blake, G. A., Cleeves, L. I. & Schwarz, K. R. Mass inventory of the giant-planet formation zone in a solar nebula analogue. *Nature Astronomy* **1**, 0130 (2017).

[46] Yoshida, T. C., Nomura, H., Furuya, K., Tsukagoshi, T. & Lee, S. A New Method for Direct Measurement of Isotopologue Ratios in Protoplanetary Disks: A Case Study of the $^{12}$CO/$^{13}$CO Ratio in the TW Hya Disk. *Astrophys. J.* **932**, 126 (2022).

[47] Maggiolo, R., Dhooghe, F., Gronoff, G. P., de Keyser, J. & Cessateur, G. Interstellar Comet 3I/ATLAS: Evidence for Galactic Cosmic-Ray Processing. *Astrophys. J.* **996**, L34 (2026).

[48] Hui, M.-T., Jewitt, D., Mutchler, M. J., Agarwal, J. & Kim, Y. Nucleus and Postperihelion Activity of Interstellar Object 3I/ATLAS Observed by the Hubble Space Telescope. *Astrophys. J.* **999**, L37 (2026).

[49] Belyakov, M. *et al.* The Volatile Inventory of 3I/ATLAS as Seen with JWST/MIRI. *Astrophys. J.* **1001**, L11 (2026).

[50] van Dokkum, P. G. Cosmic-Ray Rejection by Laplacian Edge Detection. *PASP* **113**, 1420–1427 (2001).

[51] Hutsemékers, D., Manfroid, J., Jehin, E., Zucconi, J.-M. & Arpigny, C. The $^{\{16\}}$OH/$^{18}$OH and OD/OH isotope ratios in comet C/2002 T7 (LINEAR). *Astron. Astrophys.* **490**, L31–L34 (2008).

[52] Villanueva, G. L. *et al.* A Sensitive Search for Deuterated Water in Comet 8p/Tuttle. *Astrophys. J.* **690**, L5–L9 (2009).

[53] Bockelée-Morvan, D. *et al.* Large Excess of Heavy Nitrogen in Both Hydrogen Cyanide and Cyanogen from Comet 17P/Holmes. *Astrophys. J.* **679**, L49 (2008).

[54] Biver, N. *et al.* Isotopic ratios of H, C, N, O, and S in comets C/2012 F6 (Lemmon) and C/2014 Q2 (Lovejoy). *Astron. Astrophys.* **589**, A78 (2016).

[55] Manfroid, J. *et al.* Isotopic abundance of nitrogen and carbon in distant comets. *Astron. Astrophys.* **432**, L5–L8 (2005).

[56] Hutsemékers, D. *et al.* Isotopic abundances of carbon and nitrogen in Jupiter-family and Oort Cloud comets. *Astron. Astrophys.* **440**, L21–L24 (2005).

[57] Arpigny, C. *et al.* Anomalous Nitrogen Isotope Ratio in Comets. *Science* **301**, 1522–1525 (2003).

[58] Yang, B. *et al.* Isotopic ratios in outbursting comet C/2015 ER61. *Astron. Astrophys.* **609**, L4 (2018).

[59] Bockelée-Morvan, D. *et al.* LPI Editorial Board (ed.) *A Multi-Wavelength Simultaneous Study of the Composition of the Halley-Family Comet 8P/Tuttle at the VLT.* (ed.LPI Editorial Board) *Asteroids, Comets, Meteors 2008*, Vol. 1405 of *LPI Contributions*, 8190 (2008).

[60] Jehin, E. *et al.* Deep Impact: High-Resolution Optical Spectroscopy with the ESO VLT and the Keck I Telescope. *Astrophys. J.* **641**, L145–L148 (2006).

[61] Moulane, Y. *et al.* Photometry and high-resolution spectroscopy of comet 21P/Giacobini-Zinner during its 2018 apparition. *Astron. Astrophys.* **640**, A54 (2020).

[62] Jehin, E. *et al.* LPI Editorial Board (ed.) *Optical Spectroscopy of the B and C Fragments of Comet 73P/Schwassmann-Wachmann 3 at the ESO VLT.* (ed.LPI Editorial Board) *Asteroids, Comets, Meteors 2008*, Vol. 1405 of *LPI Contributions*, 8319 (2008).

[63] Jehin, E. *et al.* *A Multi-wavelength study with the ESO VLT of comet 103P/Hartley2 at the time of the EPOXI encounter*, Vol. 2011, 1463 (2011).

[64] Jehin, E. *et al.* The Anomalous $^{14}N/^{15}N$ Ratio in Comets 122P/1995 S1 (de Vico) and 153P/2002 C1 (Ikeya-Zhang). *Astrophys. J.* **613**, L161–L164 (2004).

[65] Shinnaka, Y. *et al.* Nitrogen isotopic ratios of $NH_2$ in comets: implication for $^{15}N$-fractionation in cometary ammonia. *Mon. Not. R. Astron. Soc.* **462**, S195–S209 (2016).

[66] Shinnaka, Y. *et al. High-Dispersion Spectroscopic Observations of Comet C/2012 S1 (ISON) with the Subaru Telescope*, Vol. 46 of *AAS/Division for Planetary Sciences Meeting Abstracts*, 209.14 (2014).

[67] Rousselot, P., Jehin, E., Manfroid, J. & Hutsemékers, D. The $^{12}C_2/^{12}C^{13}C$ isotopic ratio in comets C/2001 Q4 (NEAT) and C/2002 T7 (LINEAR). *Astron. Astrophys.* **545**, A24 (2012).

[68] Shinnaka, Y. & Kawakita, H. Nitrogen Isotopic Ratio of Cometary Ammonia from High-resolution Optical Spectroscopic Observations of C/2014 Q2 (Lovejoy). *Astron. J.* **152**, 145 (2016).

[69] Stawikowski, A. & Greenstein, J. L. The Isotope Ratio C$\hat{\{}$12$\}$/C$\hat{\{}$13$\}$ in a Comet. *Astrophys. J.* **140**, 1280 (1964).

[70] Owen, T. The Isotope Ratio 12C/13C in Comet Tago-Sato (1969g). *Astrophys. J.* **184**, 33–44 (1973).

[71] Danks, A. C., Lambert, D. L. & Arpigny, C. The $^{12}C/^{13}C$ ratio in comet Kohoutek (1973f). *Astrophys. J.* **194**, 745–751 (1974).

[72] Vanysek, V. Delsemme, A. H. (ed.) *Carbon isotope ratio in comets and interstellar matter.* (ed.Delsemme, A. H.) *IAU Colloquium 39: Comets, Asteroids, Meteorites: Interrelations, Evolution and Origins*, 499–503 (1977).

[73] Wyckoff, S., Kleine, M., Peterson, B. A., Wehinger, P. A. & Ziurys, L. M. Carbon Isotope Abundances in Comets. *Astrophys. J.* **535**, 991–999 (2000).

[74] Lambert, D. L. & Danks, A. C. High-resolution spectra of C2 Swan bands from comet West 1976 VI. *Astrophys. J.* **268**, 428–446 (1983).

[75] Lis, D. C. *et al.* Spectroscopic Observations of Comet C/1996 B2 (Hyakutake) with the Caltech Submillimeter Observatory. *Icarus* **130**, 355–372 (1997).

[76] Wyckoff, S. *et al.* The 12C/ 13C Abundance Ratio in Comet Halley. *Astrophys. J.* **339**, 488 (1989).

[77] Jaworski, W. A. & Tatum, J. B. Analysis of the Swings Effect and Greenstein Effect in Comet P/Halley. *Astrophys. J.* **377**, 306 (1991).

[78] Kleine, M., Wyckoff, S., Wehinger, P. A. & Peterson, B. A. The Carbon Isotope Abundance Ratio in Comet Halley. *Astrophys. J.* **439**, 1021 (1995).

[79] Jewitt, D., Matthews, H. E., Owen, T. & Meier, R. The 12C/13C, 14N/15N and 32S/ 34S Isotope Ratios in Comet Hale-Bopp (C/1995 O1). *Science* **278**, 90–93 (1997).

[80] Ziurys, L. M. *et al.* Cyanide Chemistry in Comet Hale-Bopp (C/1995 O1). *Astrophys. J.* **527**, L67–L71 (1999).

[81] Lis, D. C. *et al.* Spectroscopic Observations of Comet C/1996 B2 (Hyakutake) with the Caltech Submillimeter Observatory. *Icarus* **130**, 355–372 (1997).

[82] Cordiner, M. A. *et al.* ALMA Autocorrelation Spectroscopy of Comets: The $HCN/H^{13}CN$ Ratio in C/2012 S1 (ISON). *Astrophys. J.* **870**, L26 (2019).

[83] Rousselot, P. *et al.* $^{12}CO^+$ and $^{13}CO^+$ fluorescence models for measuring the $^{12}C/^{13}C$ isotopic ratio in comets. *Astron. Astrophys.* **683**, A50 (2024).

[84] Müller, D. R. *et al.* High D/H ratios in water and alkanes in comet 67P/Churyumov-Gerasimenko measured with Rosetta/ROSINA DFMS. *Astron. Astrophys.* **662**, A69 (2022).

[85] Bergin, E. Q. *et al.* The Carbon Isotopic Ratio and Planet Formation. *Astrophys. J.* **965**, 147 (2024).